sciendo
ISSN 1335-8871
MEASUREMENT SCIENCE REVIEW
Journal homepage: https://content.sciendo.com

Dual-Energy Spectral Computed Tomography: Comparing True and Virtual Non Contrast Enhanced Images

Kateřina Širůčková[1], Petr Marcoň[1], Marek Dostál[2], Anna Širůčková[1], Přemysl Dohnal[1]

[1]*Brno University of Technology, Faculty of Electrical Engineering and Communication, Technicka, 12, 616 00, Brno, Czech Republic, marcon@vut.cz*
[2]*University Hospital Brno and Masaryk University, Department of Radiology and Nuclear Medicine, Jihlavska, 340/20, 625 00, Brno, Czech Republic*

Abstract: Spectral computed tomography (CT) imaging is one of several image reconstruction techniques based on the use of dual-layer CT. The intensity and attenuation of the radiation are measured in relation to different wavelengths, and such a procedure results in complex three-dimensional (3D) imaging and (pseudo) color adjustment of the soft tissue. This paper compares true non-contrast (TNC) enhanced images with virtual non-contrast (VNC) enhanced ones. Virtual native images are acquired by means of spectral computed tomography, and it has been suggested that VNCs could potentially substitute real native images to reduce significantly the total radiation dose from multiphase spectral CT. A comparison was performed by defining certain parameters that represent the difference between the measured and the calculated values in the images. The parameters included the mean value and standard deviation of the computed tomography number, signal-to-noise ratio (SNR), and contrast-to-noise ratio (CNR). All of these items were analyzed via statistical tests using *p*-value. The results are interpreted and correlated with those presented by other authors, who, however, did not make an examination on a comprehensive basis - five tissues simultaneously by using a single device. Prospectively, if analogies were found between the two types of images, it would be possible to skip the TNC image, thus markedly reducing the radiation dose for the patient.

Keywords: Biomedical data analysis, CNR, dual-layer, SNR, spectral computed tomography, statistical analysis.

1. INTRODUCTION

Computed Tomography (CT) is a modern imaging technique that utilizes X-rays. The major benefit of the method rests in the high resolution of soft tissues, tumors, thrombi, and other pathological objects. The broadest applicability is found within emergency medicine, especially thanks to the quick and effective whole-body scans. Although there are many positive aspects to the use of CT scans, the approach also brings negatives, such as a high radiation dose, technologically demanding image reconstruction, and potential allergic reactions to the iodine contrast agent.

Spectral CT imaging embodies one of several dual-layer CT image reconstruction techniques, where the lower and the upper layers of the detectors absorb high-energy and low-energy photons, respectively, thus allowing the machine to provide and detect two types of energy [1]-[3]. Simultaneously, the radiation intensity and attenuation are measured depending on various wavelengths. This then facilitates complex imaging of the soft tissue and its (pseudo) color adjustment. Due to the decomposition of the image, spectral CT can recognize voxels that contain an iodine contrast agent and determine its amount. This capability in turn enables us to create new virtual non-contrast enhanced (VNC) images calculated on the basis of the mathematical method of deconvolution [4]. In this context, a prospective topic consists of simulating the images of the whole-body scan without a contrast agent; this problem is described in source [5].

CT image reconstruction constitutes a quickly developing branch of the field being discussed. In general, a substantial amount of research has been carried out to find exact and effective methods enabling the image reconstruction process to minimize the patients' radiation exposure [6]. Currently, diverse radiation dose reduction techniques are applied in the clinical practice; shielding methods, scanning adjusted to the anatomical proportions of each patient, and segmentation of the center of interest and its immediate surroundings are representative of the procedures.

Convolution is one of the most widely used methods in the clinical practice. The filtered back projection has several limitations, such as noise processing and artifact appearance. The frequently used convolution filter attenuates the blurring caused by the back projection filter [6]-[10].

VNC imaging is a subsequent image processing technique to form non-contrast images through subtracting the iodine agent from true non-contrast images (TNCs). The procedure

DOI: 10.2478/msr-2022-0033

is unique to dual-energy CT. VNC images simulate monoenergetic CT images having 70 keV of energy without injection of a contrast agent. The quantified iodine content is converted to the number HU*, and the amount of 70 keV is subtracted from the images with the contrast agent. Theoretically, the resulting image should imitate the TNC ones (before contrast agent application) [11], [12].

VNC imaging has a potential to substitute the conventional non-contrast CT scan in multiphase imaging [13], as the delivered results are similar. VNC images can be utilized in, for example, the clinical practice of evaluating adrenal lesions [14].

Interestingly, one of the relevant articles [1] compared TNC and VNC images of various structures. The most substantial differences were found in the aorta and fat, with a higher HU* in the fat and a lower HU* in the aorta. The VNC technique thus does not seem reliable for these tissues. The average difference between the TNC and the VNC images ranged below 4 HU in all other tissue types examined (the liver, kidneys, and muscles); this indicates a high reliability of VNC images in these specimens. In total, 91.8 % of the images showed a discrepancy between the TNCs and the VNCs of less than 15 HU. The best correlation was observed in the muscular tissue. The VNC enhanced images displayed significantly less noise than the TNC ones in all of the examined structures, except for the bone tissue. The authors' primary intention was to demonstrate the variation between the TNC and the VNC techniques with respect to the HU and the HU* values; the conclusion then proposed that the VNC technique could be a promising tool for the scanning and diagnostics of kidney and liver pathologies [1].

Another article [15] evaluated the reliability of attenuation values in TNC and VNC images. The researchers measured phantoms and humans. In the phantom part of the study, virtual non-contrast images were proved to ensure reliable attenuation measurement at low, medium, and high iodine concentrations. The clinical section then established that in 91.5 % of the cases the maximum absolute difference amounted to 15 HU in the liver. The greatest discrepancies were revealed in the aorta, fat tissue, and spleen [15].

A further study examined TNC and VNC images in terms of evaluating mediastinal lymph nodes. The aim was to assess the reliability of the TNC and the VNC techniques. The absolute difference equaled or ranged below 10 HU in 65.2 % of the cases. Regarding calcification, the authors determined that calcium displays larger differences in photoelectric absorption between 80 kV and 140 kV, compared to soft tissues; such a condition then leads to a partial subtraction of the calcium signal in the formation of a VNC image. A nonhomogeneous high attenuation was observed in the superior vena cava in the VNC images, presumably because of the high concentration of the contrast agent that had remained in the vena cava. The researchers also recommended that more studies be conducted to confirm the reliability of the VNC technique in evaluating mediastinal lymph nodes [16].

Our article compares the applicability and performance of the TNC and the VNC procedures in five tissues, namely, the aorta, liver, kidneys, lungs, and fat. The results are interpreted and correlated with those presented by other authors, who, however, did not examine on a comprehensive basis - five tissues simultaneously by using a single device. Prospectively, if analogies were found between the two types of images, it would be possible to skip the TNC image, thus markedly reducing the radiation dose for the patient.

We assume diverse decomposition success rates in various tissues, as the contrast agents will be saturated differently; for this reason, we measure multiple ROIs in diverse tissues. The aim thus is to verify the accuracy achievable with VNCs and TNCs in particular tissues that are inspected during thoracic and abdominal CT scanning.

2. SUBJECT & METHODS

A. Population study

This retrospective study was approved by the local institutional board of ethics, with no informed consent required. The statistical testing included 10 male (age: 36-75; mean ± SD: 59.8 ± 13.6) and 10 female (age: 43-72; mean ± SD 58.7 ± 10.0) persons. The images acquired during CT scanning of the chest and the abdomen originated from patients in whom recordings of true and virtual native images of the aorta, liver, lungs, and fat had been available. All the patient data were completely anonymized. The scans relied on the same acquisition protocol, with the patients positioned on their backs inside the scanner and the scanning performed during exhalation to prevent organ compression.

B. Tissues investigated

The International Commission on Radiation Units and Measurements defines four basic materials in the human body: soft tissue, bone tissue, contrast agent, and metal implant.

Soft tissue is the most abundant material in the human body. These anisotropic fibrous structures are not mineralized or calcified. In a patient's body, soft tissues resemble water, due to their being composed of oxygen and hydrogen atoms [1], [17].

Bone tissue is formed through the mineralization of the intercellular mass by the calcium phosphate hydroxyapatite. Bone tissue has a higher density than soft tissue and contains elements with higher effective proton numbers. Artifacts are formed at the interfaces of bone and soft tissues; this effect arises from the different absorptions.

In some cases, the contrast between soft tissues needs to be increased; this step is performable by, for example, applying a contrast agent. In an angiographic examination, a contrast agent is essential for the diagnostics of the structure of parenchymal organs. The most frequently used contrast media contain iodine.

High corrosion resistance, chemical similarity (bone implant), long-term reliability, and excellent strength-to-weight ratio are among the greatest advantages of alloys. In healthcare, titanium alloys have found wide use. In more general terms, the share of metallic orthopedics reaches about 80 % of the materials applied; titanium alloys, however, are employed in not only orthopedics but also, for instance, dentistry, where they have gained popularity as metal tooth fillings. Regrettably, metal implants often degrade the quality of scanned images; the formation of artifacts can nevertheless

be partially prevented by choosing a suitable examination protocol. The artifacts present in the measured images have to be minimized by using post-processing methods, which are not always reliable [18]-[22]. It should also be noted that the subsequent processing, again, increases the complexity of the system.

In this paper, five types of tissues are analyzed, including those of the lungs, aorta, liver, and kidneys (Fig.1.). Fat tissue, namely, the subcutaneous tissue, was chosen as the reference, in which we assumed an almost zero absorption of the contrast agent and, by extension, a certain equivalence of the values measured in the TNCs and VNCs; the equivalence was confirmed in 80 % of the cases.

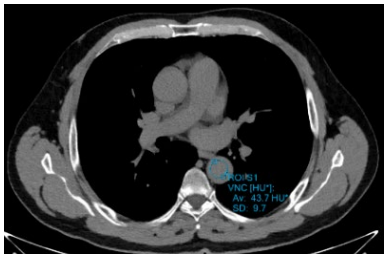

a)

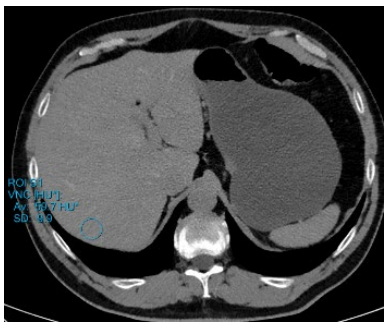

b)

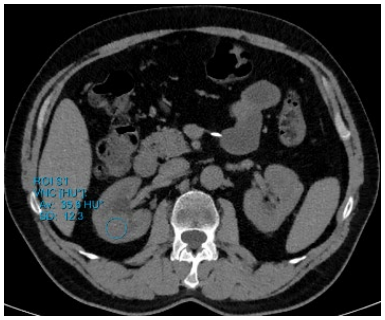

c)

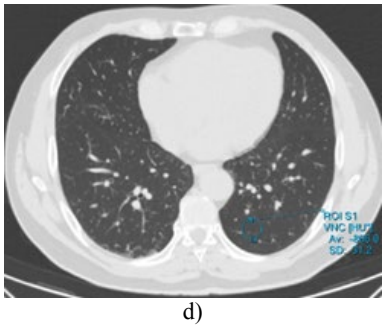

d)

Fig.1. Selected segments in the VNC images: a) the aorta, b) the liver, c) the kidneys, d) lungs.

C. Data acquisition and processing

All of the data were collected at the University Hospital Brno-Bohunice (UHB), the Department of Radiology and Nuclear Medicine. The collected data had been selected based on pre-determined requirements from September to November 2019.

To illustrate the data acquisition and processing, we propose in Fig.2. a block diagram to be described in the text below.

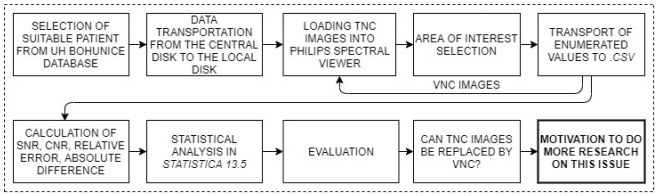

Fig.2. A workflow chart capturing the data processing, analysis, and evaluation.

A Philips IQon Spectral CT scanner with two-layer detectors was employed to acquire the images. The bottom and the upper layers of the detectors absorb high-energy and low-energy photons, respectively, allowing the machine to provide and detect two types of energy.

In all of the male and female subjects, the amount of 100 ml of type C contrast agent was applied.

During the experiment, we manually selected 200 ROIs (two ROIs in each of the twenty patients and five tissues). The size of an area of interest was set to equal 300 mm^2. For the final calculation of the SNR and CNR values in the fat, the size of an examined area was defined to be 100 mm^2. The axial layers, whose thickness amounted to 1.5 mm, were reconstructed from the sections available. The VNC images were also reconstructed in axial planes having a thickness of 1.5 mm. As VNCs and TNCs are not identical in terms of the anatomy, we had to consider the surrounding anatomies to choose very carefully another section number, performing the selection in such a manner that the number best matched the anatomy area as in the VNCs; subsequently, we inserted the ROI.

Prior to the image processing part, the images used in the experiment were transported from PACS (Picture Archiving and Communication System) of UHB to the local disc of the Clinic of Radiology and Nuclear Medicine from which they could be opened in Philips software environment. After loading the image, ROI was placed and the ratio of HU/HU* number, area (mm^2), SD, mean, and 3 curves were plotted. Histogram, scatter plot graph, and attenuation curve for energy from 45 keV to 200 keV were calculated for the ROI. The values for specific curves were exported into the *.csv file, from which the data were statistically analyzed.

The spectral reconstruction processing runs an algorithm for noise suppression using additional spectral information. This provides a significant improvement of SNR and CNR in comparison with the conventional images.

Because of the low noise from the monochromatic images on the various energy levels, these images are acceptable on all energy levels. For better vascular contrast and better visibility of the lesions, mainly low energies are used.

Contrariwise, high energies are preferred for artifact reduction. Virtual monoenergetic images (70 keV equivalent to standard CT without dual energy), pictured in Fig.3., provide an equivalent CT number on the predefined energies as the convention images scanned on 120 kVp.

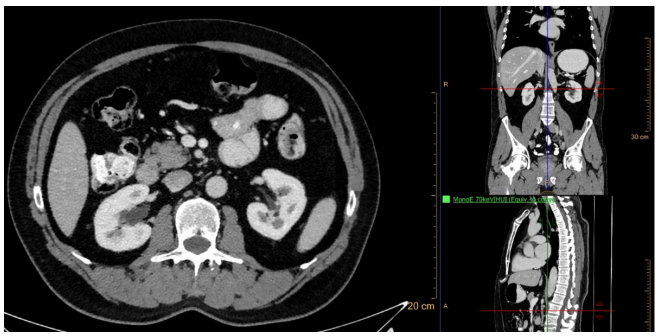

Fig.3. Illustration of Philips Spectral CT viewer environment. First image is a monoenergetic image (70 keV [HU]) that corresponds to the image acquired in a spectrum of various energies.

The examined tissues were subjects of the statistical evaluation that compared real and virtual native images. The following statistical methods were used: *p*-value, signal-to-noise ratio, contrast-to-signal ratio, absolute error, and relative error.

All data, obtained from the ROIs in the researched tissues, were tested for the Gauss distribution firstly. Required normal distribution for paired two-tailed t-test was observed only for the aorta. The other examined tissues did not demonstrate normal distribution, acquired from TNC and VNC images simultaneously, hence, a nonparametric alternative of the paired t-test, the Wilcoxon test, was chosen. The statistical level of significance α was in all cases set up on α = 0.05 which is a typical value for biological tests.

The *p*-value was used to compare the value of the test criterion with the critical values for deciding about the validity or invalidity of the null hypothesis.

Quantitative data can be described in several ways. The most basic methods contain mean, median calculation, etc. From the raw description of the data, testing of the hypothesis can be performed and statistical tests can be applied. In this article, the null hypothesis represents an absence of the difference between data selected from TNC images and their reference data from VNC images. The alternative hypothesis is the direct contradiction of the null hypothesis.

For testing of two paired dependent data sets (in our case TNC and VNC images), when the data groups are connected via the measured object (patient), paired t-test is used. Both data sets must have an equal number of measured values, which was fulfilled.

The signal-to-noise ratio (*SNR*) is used for the characterization of the image or signal quality. The *SNR* value can be quantified in decibels (dB) where the length of the noise from the signal is evaluated. *SNR* comes from the ratio of the signal power to the level of undesired signal and background noise. Generally, a higher *SNR* value indicates less noise in the image (signal) against the desirable structures.

The formula for calculating the *SNR* reads

$$SNR = \frac{mean_{\text{tissue}}}{SD_{\text{tissue}}}, \tag{1}$$

where $mean_{\text{tissue}}$ and SD_{tissue} express the mean value and standard deviation of the selected ROI, see Fig.1.-Fig.3.

The contrast-to-noise ratio (*CNR*) is a parameter used for the image quality. High *CNR* value indicates better image quality with respect to the contrast.

Formula for *CNR* calculation:

$$CNR = \frac{mean_{\text{tissue}} - mean_{\text{background}}}{SD_{\text{background}}}, \tag{2}$$

where $mean_{\text{tissue}}$ expresses mean value of examined tissue, $mean_{\text{background}}$ and $SD_{\text{background}}$ express mean value and standard deviation of background (fat).

The absolute and relative error can be also explained as a measurement deviation. It is introduced when comparing the accuracy of measurements, where it points to errors caused by image deconvolution. It is a percentage expression of the ratio of the absolute error (3) to the value of the measured quantity.

$$\Delta_{\text{TNC}} = mean_{\text{VNC}} - mean_{\text{TNC}}, \tag{3}$$

where $mean_{\text{VNC,TNC}}$ express mean value of CT number for TNC and VNC enhanced images.

The relative error is also sometimes given as a dimensionless quantity. The relative error is higher when measured (subsequently calculated) value is lower. It is given by the following formula (4).

$$\delta_{\text{TNC}} = \frac{mean_{\text{VNC}} - mean_{\text{TNC}}}{mean_{\text{TNC}}}. \tag{4}$$

3. RESULTS

The absolute errors between both image reconstructions were calculated to downsize the subtractions of positive and negative values caused by the differences between TNC and VNC enhanced images. The calculated absolute errors of the differences served as input data for mean values, standard deviation, and 95 % confidence intervals (CI) calculated separately for each tissue for all patients. CI express an estimation of the parameter with a given validity.

Table 1. Absolute errors of all examined tissues quantified in HU units, together with 95 % confidence intervals.

Tissue	Absolute error (mean ± SD)	Lower 95 % CI	Upper 95 % CI
Lungs	14.6 ± 7.3	7.1	22.0
Aorta	5.3 ± 2.3	2.9	7.7
Liver	4.2 ± 4.7	1.5	6.9
Kidneys	2.6 ± 4.5	1.8	3.4
Fat	10.5 ± 2.9	7.6	13.4

The normal distribution is matched only by the analyzed data from the aorta; the relevant value reached $p = 0.222$ in the aorta. The remaining tissues were tested by the Wilcoxon test, where the value for lungs was $p = 0.823$, and for renal tissue was $p = 0.575$. The p-value in the liver reached $p = 0.015$, therefore, in this single case the validity of the null hypothesis was rejected.

The statistical tests proved that there is no statistically significant difference in the measured values for the TNC and the VNC images in three out of the four cases. The difference was not confirmed for the aorta, lungs, and kidneys. Liver tissue alone shows a statistically significant difference between TNC and VNC images for 20 tested patients.

The attenuation of the TNC and the VNC is presented within Table 2., directly in HU. Statistical variables, namely median and IQR (Inter Quartile Range), are given for the tissues studied.

Fig.4. is a graph with the *SNR* value of the aorta, kidney, and liver tissue. The *SNR* value was calculated from the ROIs in the TNC images according to formula (1). Similarly, the *SNR* values for VNC images were acquired from the identical ROIs. When *SNR* was compared, VNC images manifested higher values than TNC images. However, the values of VNC and TNC images for lung tissue are almost identical, which is not correct in this case and it is caused by the error of bias due to the small sample size of the patients. Any extreme deviations did not appear in comparison to the final interpretation of the results in Fig.4. and Fig.5.

After the *CNR* calculation for all tissues, the dependency of the specific tissues was studied closer. The graph in Fig.6. shows obviously that VNC images reach higher *CNR* values than TNC images. In the case of the lung tissue, displayed in Fig.7., the results are opposite, thus the VNC image attains lower values than the TNC image.

Table 2. Absolute errors of all examined tissues quantified in HU units, together with 95 % confidence intervals.

		$TNC - VNC$	$Abs(TNC - VNC)$	$\frac{Abs(TNC - VNC)}{Abs(TNC)}.100\ \%$	$\frac{Abs(TNC - VNC)}{Abs(TNC)}.100\ \%$
Lung	Median	-1.00	8.20	0.9524	-0.1109
	IQR	16.675	18.025	2.0695	1.9243
Aorta	Median	-1.60	3.80	9.6971	-4.8392
	IQR	6.775	7.275	16.3904	18.2032
Liver	Median	-1.10	1.60	2.8313	-1.9132
	IQR	4.375	5.075	8.6509	8.6824
Kidney	Median	-0.35	2.90	10.3373	-1.0689
	IQR	6.125	2.775	9.5194	18.7604

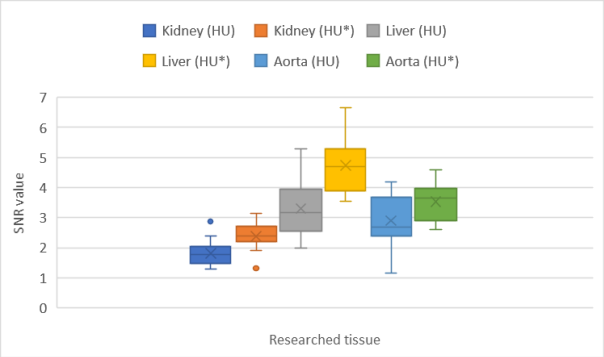

Fig.4. Box plot of TNC (HU) and VNC (HU*) based on the *SNR* evaluation from aorta, kidney, and liver tissue.

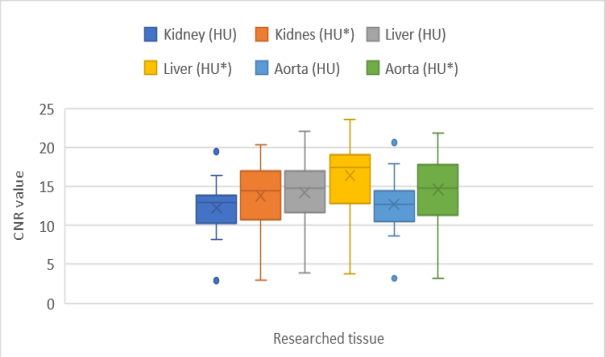

Fig.6. Box plot for TNC (HU) and VNC (HU*) based on the *CNR* evaluation from aorta, kidney, and liver tissue.

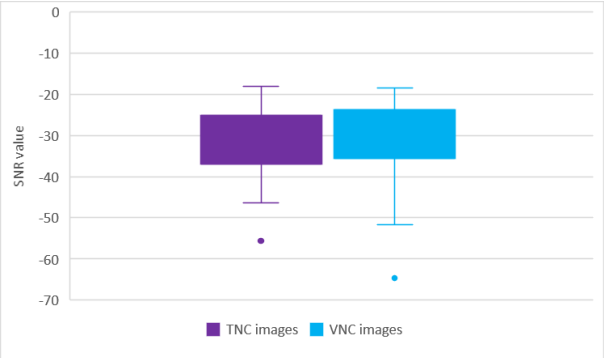

Fig.5. *SNR* values for lung tissue.

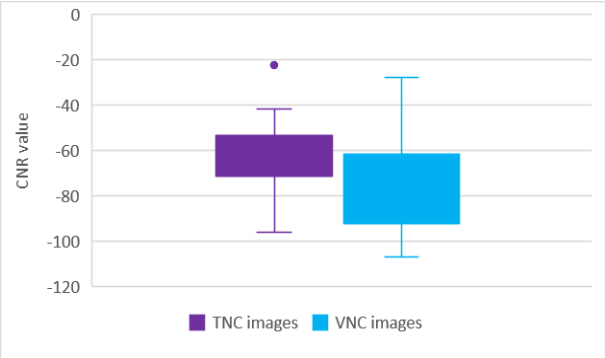

Fig.7. Box plot for TNC (HU) and VNC (HU*) based on the *CNR* evaluation from lung tissue.

Fig.8. represents the variability of relative error values of processing caused by the deconvolution of VNC enhanced images. The x axis shows the patients' order and the y axis gives the percentage value of the relative error. The mean value of fat underestimation (green) is (-9.5 ± 6.09) %. Yellow marked liver tissue acquires mean values of relative error (7.23 ± 13.01) %. The aorta (orange) and kidney (blue) reach values of (9.58 ± 26.4) % and (-1.31 ± 9.99) %. The most accurate measurement was performed within the lung tissue (purple) as it shows the lowest relative errors (0.04 ± 2.66) %.

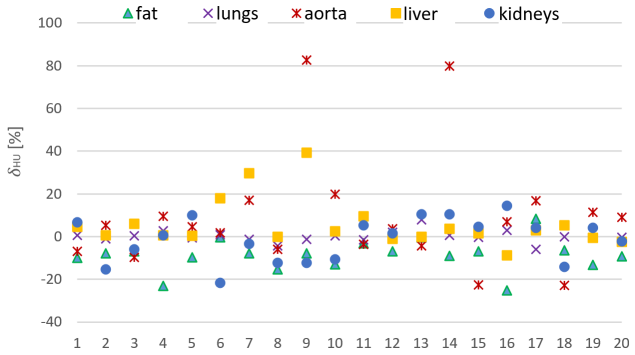

Fig.8. A graph of the relative error of the VNC calculation for all tissues.

4. Discussion and Conclusion

This paper compares real and virtual native images acquired via spectral computed tomography. The actual comparison was carried out by using several prominent parameters (absolute error, relative error, signal-to-noise ratio, contrast-to-signal ratio). Moreover, statistical testing was employed to respond to the tested null hypothesis, which had predicted zero difference between TNC and VNC values.

The difference of the TNC and the VNC image values was tested by means of the paired sample t-test and the Wilcoxon test. According to the measured average values for the lungs, aorta, and kidneys, the TNC and the VNC images do not show statistically significant differences. The analyzed data from the liver region reached $p = 0.015$, demonstrating a value lower than the statistical level of significance α. The values that influenced the resulting interpretation of the null hypothesis occurred in 25 % of the 20 patients.

The difference of 15 HU between the TNC and the VNC enhanced images is acceptable [1], [4], [14]. The mean difference of up to 15 HU presented in article [1] was reached in 91.8 % of the subjects. In our research, the mean difference of all tested tissues did not reach higher, thus remaining below 15 HU in all of the cases. The results may have been influenced by the contrast agent, whose concentration equaled 350 mg/l (OMN350 and OPT350), compared to the ULTR370 agent referred to in source [1]. An enhancement in the quality the results could be achieved through the ever improving capabilities of the medical devices, together with more efficient image processing; at this point, however, we need to emphasize that the referenced study [1] was released in July 2018 and is therefore still rather new.

At this stage, we will discuss the specific results in more detail. The kidneys do not show a difference exceeding 15 HU; hence, the virtual non-contrast technique appears to be a promising tool for the imaging of this tissue structure. Such a proposition is proved also by the authors of article [14], where VNC enhanced images are employed mainly in the evaluation of adrenal lesions. Lung tissues exhibit greater differences in HU units in 30 % of the cases. This statement is also confirmed by the fact that the lung tissue is seldom studied in combination with a virtual non-contrast technique. This deficiency may arise from the fact that lungs do not saturate significantly with the contrast medium, and, due to deconvolution, the amount of the applied contrast medium does not have to be considered (as is the case with the aorta, for example). In two of the twenty patients, i.e., 10 % of the subjects, the difference appeared to exceed 15 HU in the aorta and the liver, yet the median attains 1.6 HU in the liver and 3.35 HU in the aorta; such an outcome is regarded as a negligible difference in, for instance, article [15].

Concerning the image noise level, we characterized this issue by applying the parameters SNR and CNR; interestingly, the VNC images contained less noise than the TNC ones. In more concrete terms, this claim was supported by 83.75 % of the images evaluated with the SNR and 60 % of those classified via the CNR, assuming VNCs. The values calculated in the liver were the least noisy.

The definition of the relative error in the VNC enhanced images, relating to tissues from all of the patients, ranges among other parameters to facilitate evaluating the relevant VNC–TNC divergences. Regarding this evaluation, the most accurate tissue was that of the lungs (0.04 ± 2.66) %, while the least accurate one stemmed from the aorta, with the mean values of (9.58 ± 26.4) %. The higher error rate in the aorta was probably caused by an improper release of the contrast agent (i.e., bolus tracking); the release process is patient-specific. The aorta tissue is also the only flowing type we have examined, and this aspect may have played a certain role in the actual evaluation.

Some of our results confirm the outcomes of study [27], which focuses on abdominal tissues (the liver, spleen, kidney, muscle, and fat). Similarly, the results of the research outlined in article [3], whose authors analyzed images for aortic intramural hematoma (IMH) diagnosing, partly correlate with ours. By extension, source [2] compares VNCs and TNCs in lungs and phantom samples. Our study expands on the results of these articles as regards the kidney tissue; the results suggest that VNC images embody a reliable alternative to TNC-based imaging of the kidneys. Otherwise, in the aorta, the analysis of the scans revealed a significant difference between the TNC and the VNC images, pointing to the necessity to acquire both types.

Imaging via the VNC technique is a promising procedure for the everyday clinical routine. One of the greatest advantages rests in the permanent availability of VNC images, which, in combination with the two-layer spectral CT, leads to an essential reduction of the radiation exposure and an improvement in the diagnostic value of the one-phase CT scanner. Simultaneously, however, we need to mention possible disadvantages, such as deconvolution failures. This problem, more specifically, produces a lack of credible natives, rendering the whole examination potentially de facto useless, as changes in the HU before and after an application of the contrast agent cannot be compared.

Another benefit lies in the very precise anatomical agreement between VNCs and the contrast examination (in a TNC, the patient may exhale or move during the phases, so there may be a slight shift between the native and the postcontrast). This condition then accelerates the examination procedures.

In TNC image substitution, it is vital to review the effect of using the VNC technique on a pathological tissue. The reliability of the deconvolution algorithms in calcified tissues was confirmed to be fully individual, depending on the actual tissue.

In the context of the substitution, an essential advantage is a reduction of the X-ray dose. Conversely, a major disadvantage consists in that some anatomical areas (the kidneys, heart) will make the VNC differ from the TNC, as there is a substantial amount of contrast [28]. Upon quick reading, the number of patients in our research may be interpreted as rather low; however, it should also be noted that the described examination is very special, and thus we currently cannot collaborate with enough subjects to meet more demanding comparison criteria. Importantly, a similar number of patients, 21, is reported in an article released in 2018 [2]. Our study is unique in that it focuses on 5 tissues in each patient, and a total of 200 ROIs are processed and evaluated.

As regards the radiation, let us stress that some of the previous studies [1], [23]-[25] showed an average effective dose of 8.4 – 8.8 mSv in abdominal, pelvic, and thoracic CT. In three-phase scanning, the radiation dose is generally estimated to be around 26.4 mSv. If the future studies propose a viable substitution for the TNC image, the radiation dose in a patient will drop 1/3 (in three-phase scanning). Such a change would positively affect the concrete single radiation dose, eventually producing a mere 17.6 mSv [26].

ACKNOWLEDGMENT

The preparation of this paper was assisted by the general student development project in progress at Brno University of Technology. Supported by the Ministry of Health, Czech Republic - conceptual development of research organization (FNBr, 65269705).

REFERENCES

[1] Sauter, A.P., Muenzel, D., Dangelmaier, J., Braren, R., Pfeiffer, F., Rummeny, E.J., Noël, P.B., Fingerle, A.A. (2018). Dual-layer spectral computed tomography: Virtual non-contrast in comparison to true non-contrast images. *European Journal of Radiology*, 104, 108-114. https://doi.org/10.1016/j.ejrad.2018.05.007

[2] Hua, C.H., Shapira, N., Merchant, T.E., Klahr, P., Yagil, Y. (2018). Accuracy of electron density, effective atomic number, and iodine concentration determination with a dual-layer dual-energy computed tomography system. *Medical Physics*, 45 (6), 2486-2497. https://doi.org/10.1002/mp.12903

[3] Si-Mohamed, S., Dupuis, N., Tatard-Leitman, V. et al. (2019). Virtual versus true non-contrast dual-energy CT imaging for the diagnosis of aortic intramural hematoma. *European Radiology*, 29, 6762-6771. https://doi.org/10.1007/s00330-019-06322-5

[4] Fieselmann, A., Kowarschik, M., Ganguly, A., Hornegger, J., Fahrig, R. (2011). Deconvolution-based CT and MR brain perfusion measurement: Theoretical model revisited and practical implementation details. *International Journal of Biomedical Imaging*, 2011, 467563. https://doi.org/10.1155/2011/467563

[5] Coche, E. (2019). *Spectral CT Clinical Case Collection: Technical Aspects of Spectral CT*. Philips Health System.

[6] Murphy, A., Haouimi, A. (2020). Image reconstruction (CT). *Radiopaedia.org*. https://doi.org/10.53347/rID-51829

[7] Klosowski, G., Rymarczyk, T., Kozlowski, E. (2019). Tomographic image correction with noise reduction algorithms. *MATEC Web of Conferences*, 252, 09001. https://doi.org/10.1051/matecconf/201925209001

[8] Tan, L.-G., Xu, C., Wang, Y.-F., Wei, H.-N., Zhao, K., Song, S.-M. (2020). Gaussian recursive filter for nonlinear systems with finite-step correlated noises and packet dropout compensations. *Measurement Science Review*, 20 (2), 80-92. https://doi.org/10.2478/msr-2020-0011

[9] Zou, X., Li, K., Pan, B. (2020). The effect of low-pass pre-filtering on subvoxel registration algorithms in digital volume correlation: A revisited study. *Measurement Science Review*, 20 (5), 202-209. https://doi.org/10.2478/msr-2020-0025

[10] Andris, P., Frollo, I. (2020). Sensitivity analysis of the simply noise-matched receiving coil for NMR experiments. *Measurement Science Review*, 20 (5), 236-240. https://doi.org/10.2478/msr-2020-0030

[11] Hsu, C.C.-T., Kwan, G.N.C., Singh, D., Pratap, J., Watkins, T.W. (2016). Principles and clinical application of dual-energy computed tomography in the evaluation of cerebrovascular disease. *Journal of Clinical Imaging Science*, 6 (27). https://doi.org/10.4103/2156-7514.185003

[12] Nicolaou, S., Liang, T., Murphy, D.T., Korzan, J.R., Ouellette, H., Munk, P. (2012). Dual-energy CT: A promising new technique for assessment of the musculoskeletal system. *American Journal of Roentgenology*, 199 (5 Suppl), S78-S86. https://doi.org/10.2214/ajr.12.9117

[13] Murphy, A., Worsley, C. (2021). Virtual non-contrast imaging. *Radiopaedia.org*. https://doi.org/10.53347/rID-66311

[14] Ananthakrishnan, L., Rajiah, P., Ahn, R., Rassouli, N., Xi, Y., Soesbe, T.C., Lewis, M.A., Lenkinski, R.E., Leyendecker, J.R., Abbara, S. (2017). Spectral detector CT-derived virtual non-contrast images: Comparison of attenuation values with unenhanced CT. *Abdominal Radiology*, 42 (3), 702-709. https://doi.org/10.1007/s00261-016-1036-9

[15] Toepker, M., Moritz, T., Krauss, B., Weber, M., Euller, G., Mang, T., Wolf, F., Herold, C.J., Ringl, H. (2012). Virtual non-contrast in second-generation, dual-energy computed tomography: Reliability of attenuation values. *European Journal of Radiology*, 81 (3), e398-e405. https://doi.org/10.1016/j.ejrad.2011.12.011

[16] Yoo, S.Y., Kim, Y., Cho, H.H., Choi, M.J., Shim, S.S., Lee, J.K., Baek, S.Y. (2013). Dual-energy CT in the assessment of mediastinal lymph nodes: Comparative study of virtual non-contrast and true non-contrast images. *Korean Journal of Radiology*, 14 (3), 532-539. https://doi.org/10.3348/kjr.2013.14.3.532

[17] Choi, W.-J., Choi, T.-S. (2013). Automated pulmonary nodule detection system in computed tomography images: A hierarchical block classification approach. *Entropy*, 15 (2), 507-523. https://doi.org/10.3390/e15020507

[18] Bartusek, K., Gescheidtova, E., Mikulka, J. (2010). Data processing in studying biological tissues, using MR imaging techniques. In *33th International Conference on Telecommunications and Signal Processing*, 171-175.

[19] Mikulka, J., Burget, R., Říha, K., Gescheidtová, E. (2013). Segmentation of brain tumor parts in magnetic resonance images. In *2013 36th International Conference on Telecommunications and Signal Processing (TSP)*. IEEE, 565-568. https://doi.org/10.1109/TSP.2013.6613997

[20] Beigelman-Aubry, C., Hill, C., Guibal, A., Savatovsky, J., Grenier, P.A. (2005). Multi-detector row CT and postprocessing techniques in the assessment of diffuse lung disease. *RadioGraphics*, 25 (6), 1639-1652. https://doi.org/10.1148/rg.256055037

[21] Flohr, T., Ohnesorge, B. (2007). Image visualization and post-processing techniques. In *Multi-slice and Dual-source CT in Cardiac Imaging*. Springer, 151-177. https://doi.org/10.1007/978-3-540-49546-8_6

[22] Xiang, Z., Huang, F., Liang, C., Xu, X., Tan, L. (2008). Application of imaging postprocessing of spiral CT in the staging of lung cancer. *The Chinese-German Journal of Clinical Oncology*, 7 (5), 254-258. https://doi.org/10.1007/s10330-008-0026-y

[23] Su, K.-H., Kuo, J.-W., Jordan, D.W. et al. (2018). Machine learning-based dual-energy CT parametric mapping. *Physics in Medicine & Biology*, 63 (12), 125001. https://doi.org/10.1088/1361-6560/aac711

[24] Rassouli, N., Chalian, H., Rajiah, P., Dhanantwari, A., Landeras, L. (2017). Assessment of 70-keV virtual monoenergetic spectral images in abdominal CT imaging: A comparison study to conventional polychromatic 120-kVp images. *Abdominal Radiology*, 42, 2579-2586. https://doi.org/10.1007/s00261-017-1151-2

[25] McCollough, C.H., Leng, S., Yu, L., Fletcher, J.G. (2015). Dual- and multi-energy CT: Principles, technical approaches, and clinical applications. *Radiology*, 276 (3), 637-653. https://doi.org/10.1148/radiol.2015142631

[26] Padole, A., Singh, S., Lira, D., Blake, M.A., Pourjabbar, S., Khawaja, R.D.A., Choy, G., Saini, S., Do, S., Kalra, M.K. (2015). Assessment of filtered back projection, adaptive statistical, and model-based iterative reconstruction for reduced dose abdominal computed tomography. *Journal of Computer Assisted Tomography*, 39 (4), 462-467. https://doi.org/10.1097/rct.0000000000000231

[27] Jamali, S., Michoux, N., Coche, E., Dragean, C.A. (2019). Virtual unenhanced phase with spectral dual-energy CT: Is it an alternative to conventional true unenhanced phase for abdominal tissues? *Diagnostic and Interventional Imaging*, 100 (9), 503-511. https://doi.org/10.1016/j.diii.2019.04.007

[28] Lazar, M., Ringl, H., Baltzer, P. et al. (2020). Protocol analysis of dual-energy CT for optimization of kidney stone detection in virtual non-contrast reconstructions. *European Radiology*, 30, 4295-4305. https://doi.org/10.1007/s00330-020-06806-9

Received December 29, 2021
Accepted July 04, 2022